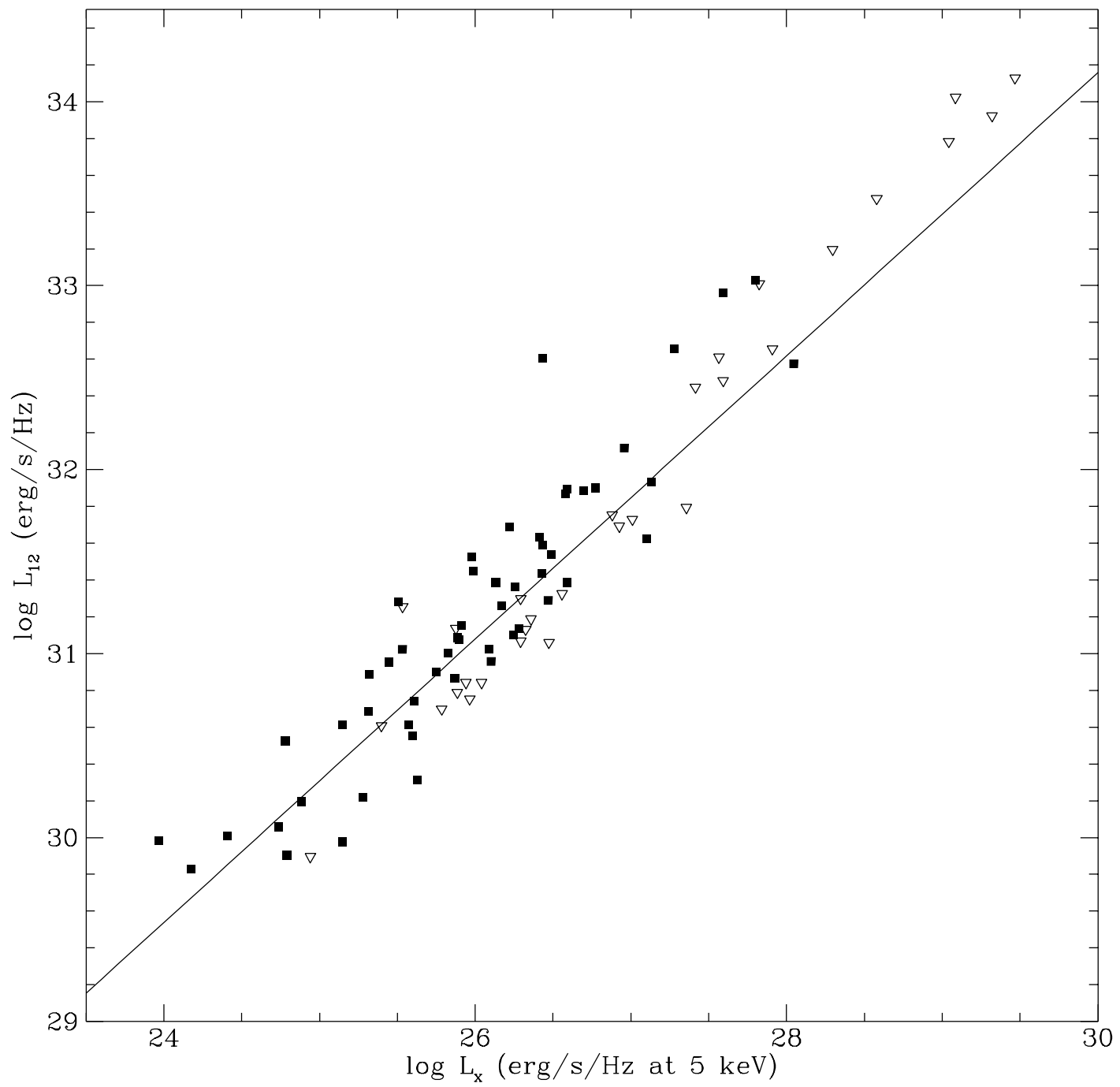


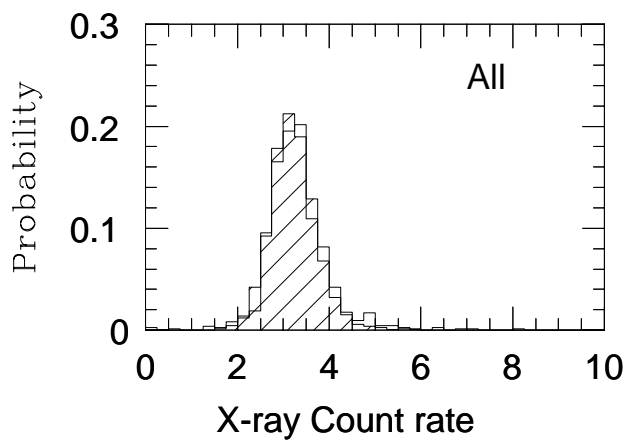
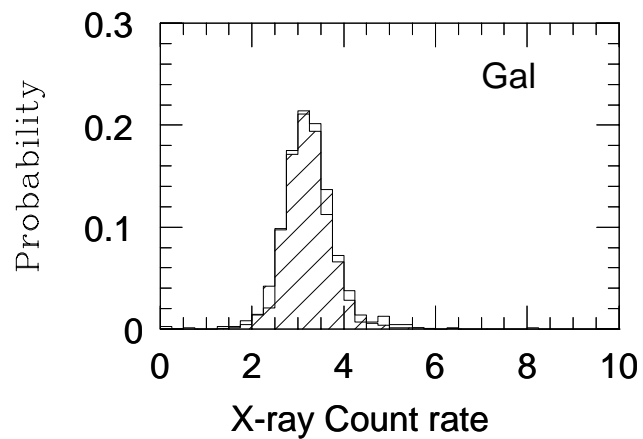
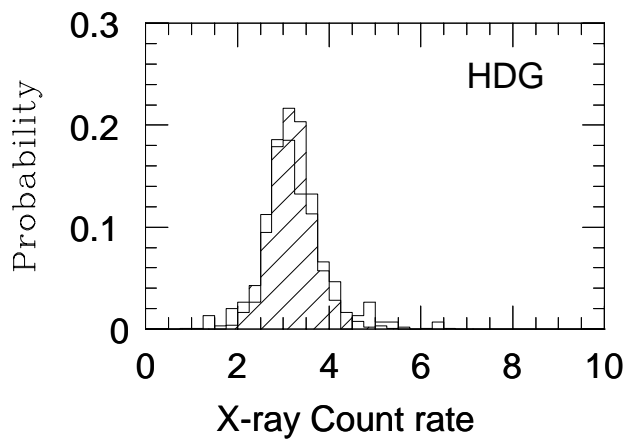
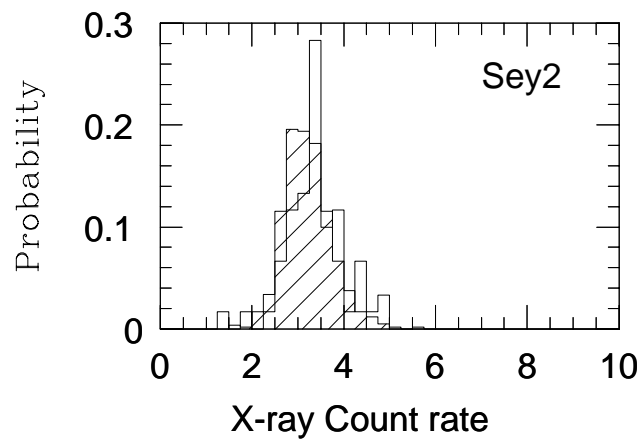
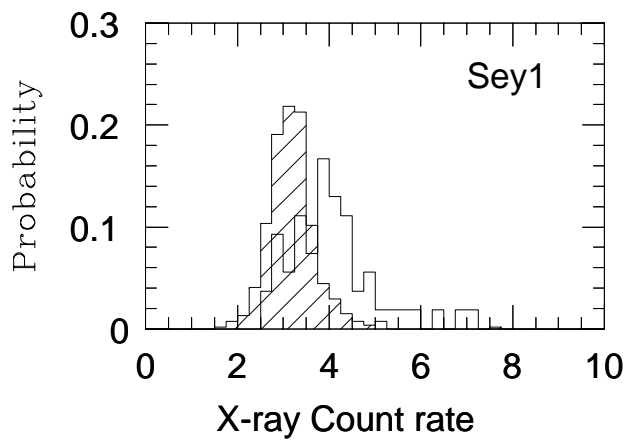
**Table 1.** Results of the search of  $f_X/f_{12\mu}$  for different subsamples. Error ranges and upper limits quoted at 95 per cent confidence. Estimates of 2-10 keV volume emissivities for the various samples.

Sample	No. Sources	X-ray Band	Significance (%)	$f_X/f_{12\mu}$
Seyfert 1	54	Total	> 99.9999	$(1.4_{-0.4}^{+1.1}) \times 10^{-6}$
Seyfert 1 $L_{12\mu} < 10^{30}$	33	Total	> 99.999	$(1.2_{-0.4}^{+1.8}) \times 10^{-6}$
Seyfert 1 $L_{12\mu} > 10^{30}$	21	Total	~ 95	$(1.6_{-1.2}^{+1.2}) \times 10^{-6}$
Seyfert 1	54	Hard	> 99	$(1.4_{-0.8}^{+1.2}) \times 10^{-6}$
Seyfert 2	59	Total	~ 95	$(2.0_{-1.5}^{+4.5}) \times 10^{-7}$
Seyfert 2	59	Hard	~ 85	$(3_{-3}^{+4}) \times 10^{-7}$
Hot Dust Galaxies	152	Total	< 70	$< 1.0 \times 10^{-7}$
Galaxies	721	Total	< 70	$< 0.8 \times 10^{-7}$
All	835	Total	> 95	$(0.8_{-0.6}^{+0.6}) \times 10^{-7}$



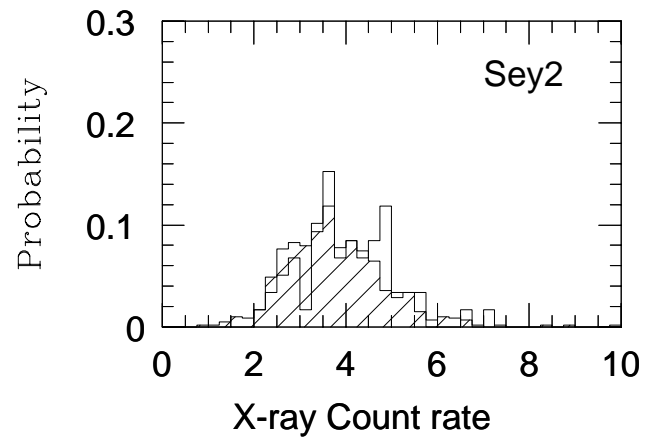
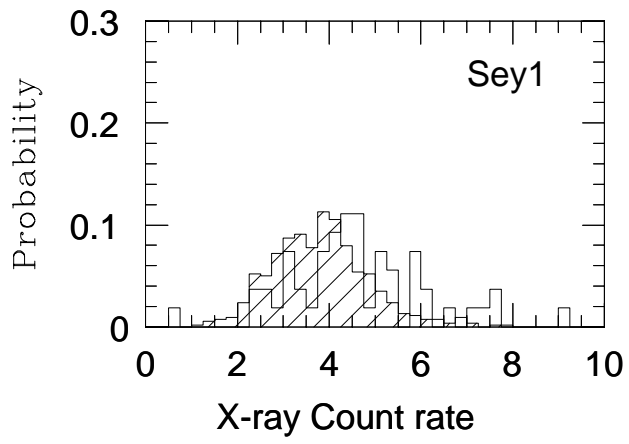
**Table 2.** Cross-Correlation Function of different galaxy catalogues with the A2 sky map and inferred  $\nu$  errors and upper limits refer to the 95% level (obtained by bootstrapping techniques).

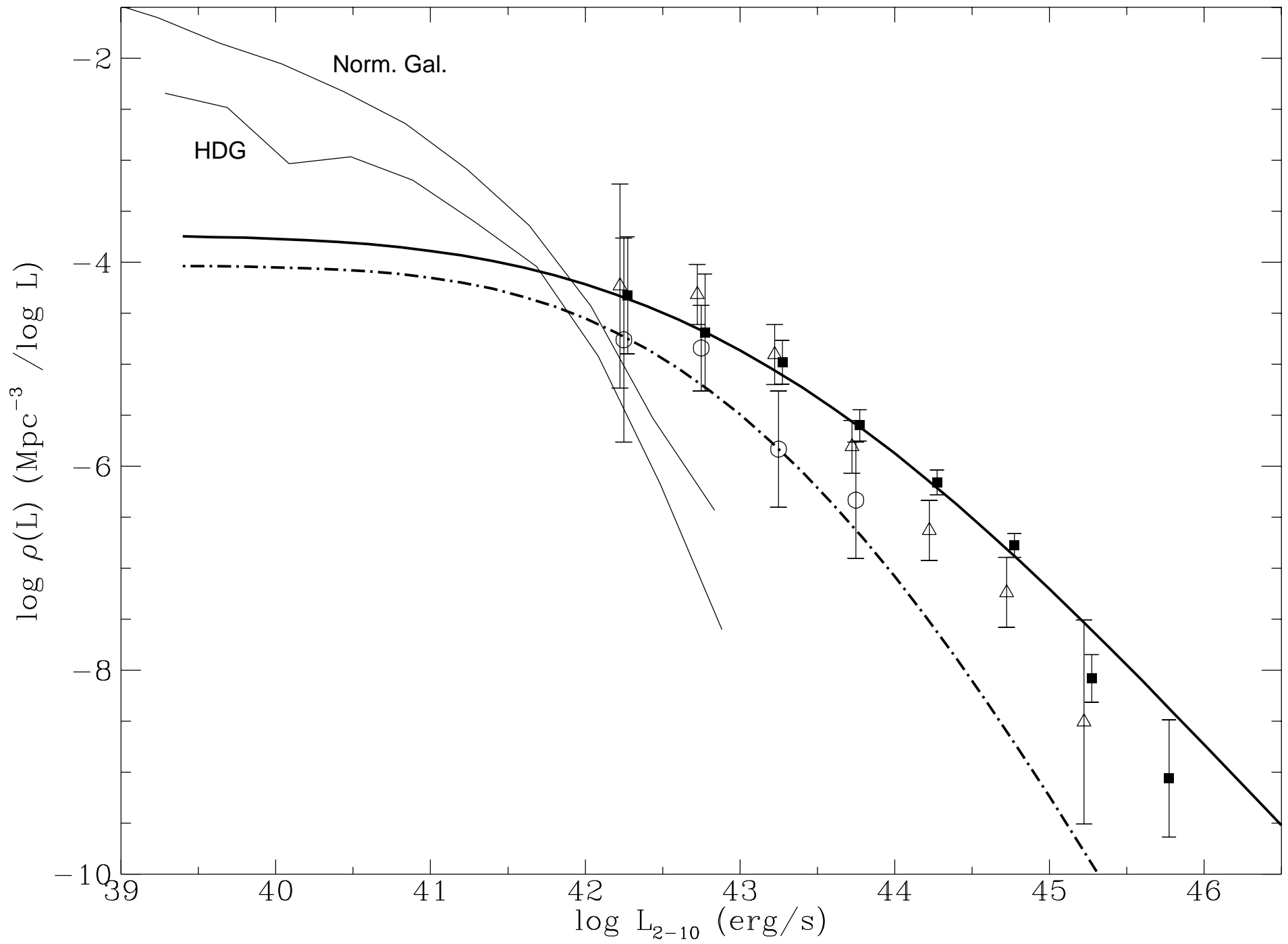
Sample	Source density (sources/beam)	$R_{\star}$ (Mpc)	$R_{clus}$ (Mpc)	CCF
Seyfert 1	$1.04 \times 10^{-2}$	$108_{-21}^{+28}$	$0.6_{-0.1}^{+0.1}$	$(1.14_{-0.3}^{+1.1}) \times 10^{-3}$
Seyfert 2	$1.15 \times 10^{-2}$	$94_{-21}^{+32}$	$0.7_{-0.1}^{+0.1}$	$(3.1_{-2.2}^{+4.8}) \times 10^{-2}$
Hot Dust Galaxies	$2.9 \times 10^{-2}$	$68_{-8}^{+9}$	$2.4_{-0.2}^{+0.2}$	$(1.7_{-15}^{+11}) \times 10^{-3}$
Galaxies	$1.4 \times 10^{-1}$	$57_{-5}^{+5}$	$12_{-0.5}^{+0.5}$	$(0.3_{-15}^{+11}) \times 10^{-3}$
All	$1.6 \times 10^{-1}$	$61_{-1}^{+5}$	$13.5_{-0.5}^{+0.5}$	$(9.0_{-9.6}^{+13}) \times 10^{-3}$



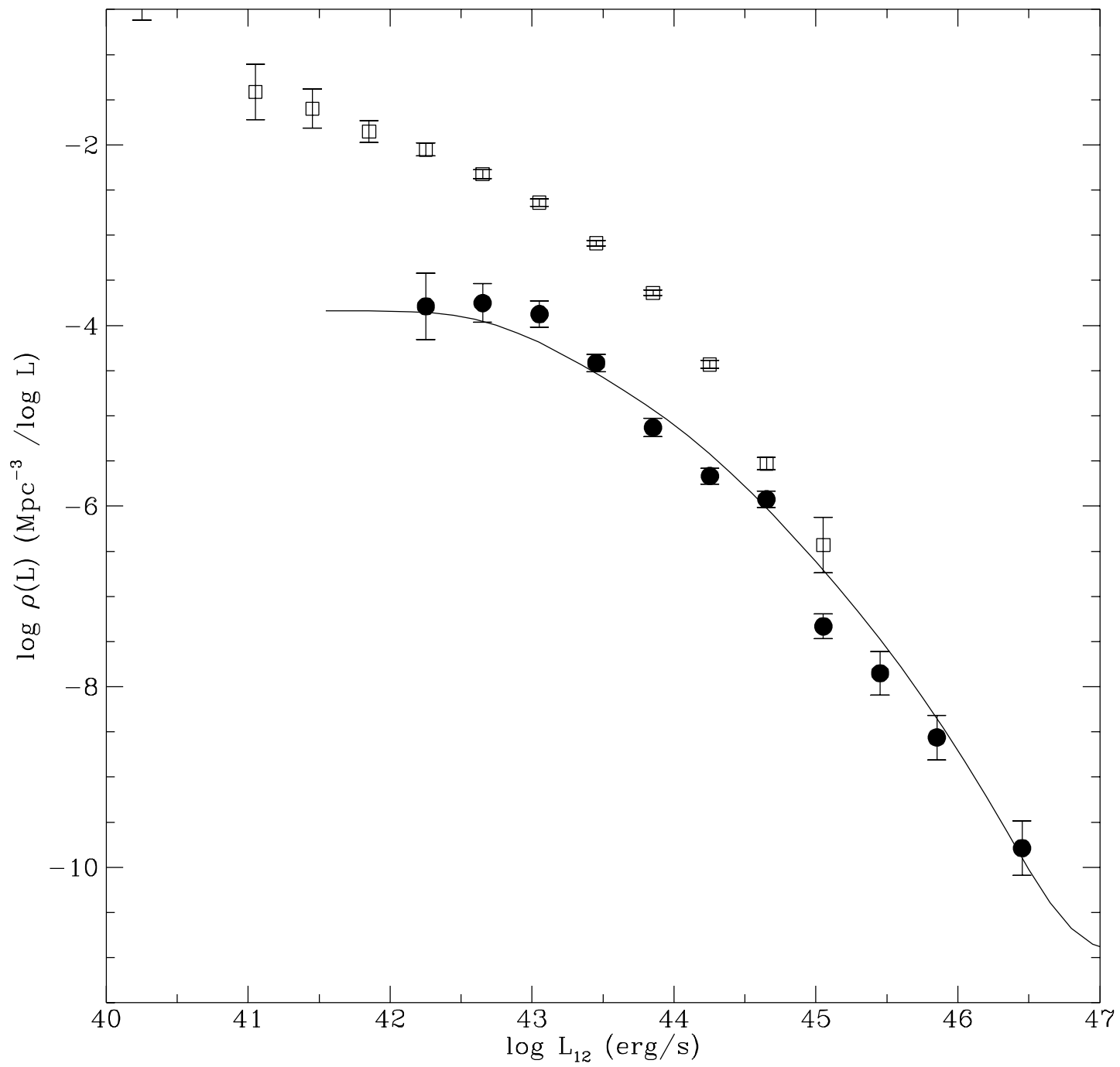
**Table 3.** Non linear fits to the  $L_X$  vs  $L_{12}$  relation for Seyfert 1 galaxies selected at  $12\mu\text{m}$  as defined by eq. (2). For the listed values of the slope  $b$ , the normalisation  $a$  is fitted by means of the IDA.

$b$	$a$
1.20	$-12.0 \pm 0.25$
1.25	$-13.6 \pm 0.25$
1.30	$-15.1 \pm 0.25$
1.40	$-18.2 \pm 0.25$









HARD X-RAY EMISSION FROM EXTRAGALACTIC *IRAS*  $12\mu\text{m}$  SOURCES:  
CONSTRAINTS ON THE UNIFIED AGN MODEL  
AND THE SYNTHESIS OF THE X-RAY BACKGROUND

XAVIER BARCONS

Instituto de Física de Cantabria (Consejo Superior de Investigaciones Científicas -  
Universidad de Cantabria), 39005 Santander, Spain

Electronic mail: barcons@astro.unican.es

ALBERTO FRANCESCHINI, GIANFRANCO DE ZOTTI

Osservatorio Astronomico di Padova. Vicolo dell' Osservatorio 5, 35122 Padova, Italy

Electronic mail: franceschini, dezotti@astrpd.pd.astro.it

LUIGI DANESE

SISSA - International School for Advanced Studies, Strada Costiera 11, 34014 Trieste, Italy

Electronic mail: danese@astrpd.pd.astro.it

AND

TAKAMITSU MIYAJI\*

Code 666, NASA/Goddard Space Flight Center, Greenbelt, MD 20771, USA, and  
Department of Astronomy, University of Maryland, College Park, Maryland 20742, USA

Electronic mail: miyaji@rosat.mpe-garching.mpg.de

---

\* Present address: Max-Planck-Institut für Extraterrestrische Physik, Postfach 1603,  
D-85740 Garching bei München, Germany

## ABSTRACT

We analyze the 2–10 keV X-ray emission of complete samples of AGN and galaxies selected at  $12\mu\text{m}$  and recently compiled by Rush, Malkan & Spinoglio (1993). The content in active galaxies of the  $12\mu\text{m}$  sample is indeed much larger and less biased against low luminosity and ‘hidden’ active nuclei than for samples selected at other wavelengths. As a necessary complement we also study the IR emissivity of the largest sample of hard X-ray selected AGN (Grossan 1992). Our purposes are to probe the unified scheme of active nuclei and to evaluate the local X-ray volume emissivity of low luminosity and ‘hidden’ AGN.

Two methods are used in our analysis to search for X-ray emission in the HEAO-1 A2 all-sky maps from the extragalactic sources contained in the extended  $12\mu\text{m}$  sample: an X-ray Intensity Distribution Analysis (IDA) around the known positions of the sources and a cross-correlation function (CCF) analysis between galaxy densities and X-ray intensities in the high galactic latitude sky ( $|b| > 25^\circ$ ), where the catalogue is  $> 98$  per cent complete.

The joint analysis of the X-ray selected and  $12\mu\text{m}$  selected samples enable us to define the relationship between the X-ray and the mid-IR emissions of Seyfert nuclei. In particular it turns out that congruence is found between the hard X-ray and mid-IR Seyfert 1 nuclear luminosity functions if a non-linear relation  $L_{12\mu} \propto L_{5\text{keV}}^{0.8}$  is assumed with appropriate dispersion. Although this result is easily explained by circum-nuclear dust re-radiation as the main source of the mid-IR emission, nonetheless it argues against the simplest version of the unified model for active nuclei.

We confirm that X-ray emission is basically restricted to AGN, Seyfert 1’s being much more powerful emitters than Seyfert 2’s. We find no signal of X-ray emission for the remaining galaxies selected at  $12\mu\text{m}$ , not even for those having a flat far-infrared spectrum, which would be prime candidates to host hidden AGN. Our result on the local volume emissivity of the Seyfert 1’s is fully consistent with those derived from studies of the hard X-ray luminosity function. However the 95% upper limits to the local emissivity we derive for the Seyfert 2 class and for the most likely ‘hidden’ AGN candidates, severely constrain (and in some cases exclude) models of the X-ray background based on the unified

Seyfert scheme.

We also find that less than  $\sim 20\%$  of Seyfert 1-like AGN and less than  $\sim 50\%$  of Seyfert 2-like AGN can be ‘hidden’ in the non-Seyfert galaxy samples assuming that the X-ray to  $12\mu\text{m}$  flux ratios measured in the  $12\mu\text{m}$  selected samples can be considered typical for these classes of objects. In this case, the number ratio of Seyfert 2 to Seyfert 1 galaxies ranges from 1 to 2.

*Subject headings:* Galaxies: general, active – Infrared: galaxies – X-rays: general, galaxies, diffuse radiation

## 1. INTRODUCTION

The unified Seyfert scheme (Antonucci & Miller 1985; see Antonucci 1993 for a comprehensive review) predicts that active nuclei are surrounded by torus-like opaque structures of gas and dust. Depending on the line of sight to the nuclei, the UV and optical broad line emitting regions may be obscured or not and the objects can be classified as broad- or narrow-line AGN.

Two issues of the unified scheme are relevant to our study: the nature of the IR emission and the absorption and reprocessing of the primary X-ray nuclear emission. In the unified picture the most natural explanation of the near and mid-IR emission of Seyfert galaxies is re-radiation of the primary optical-UV radiation by thermal dust in the torus around the active nucleus (see e.g. Pier & Krolik 1992; Granato & Danese 1994). The near and mid-IR radiation from AGN is expected to be mildly anisotropic in this context (Granato & Danese 1994). However, the selection bias against obscured (type 2) and ‘hidden’ AGN is likely to be less severe here than in the  $< 10$  keV X-ray domain where the flux transmitted through the obscuring torus will be suppressed by a factor of several orders of magnitude (Krolik, Madau & Zycki 1994). The unified picture also predicts heavy absorption in the X-ray spectra of the narrow-line AGN with respect to the broad-line ones (see e.g. Krolik, Madau & Zycki 1994). As a matter of fact, *Ginga* observations revealed high absorbing column densities ( $N_{HI} \sim 10^{23} - 10^{25} \text{ cm}^{-2}$ ) in many Seyfert 2 galaxies (Awaki et al 1991), whereas Seyfert 1 X-ray spectra exhibit moderate to low or even no absorption. Active objects surrounded by Compton-thick tori with even higher column densities are also expected in the unified model (Antonucci 1993).

On the other hand there are evidences that the simplest version of the unified model is not valid (Lawrence 1991; Mulchaey, Mushotzky & Weaver 1992; Antonucci 1993) and that effects other than the orientation of the line of sight must be called for to explain the difference between type 1 and type 2 AGN. In particular the luminosity of the central nucleus may be a crucial parameter in a more refined model. In this context much can be learnt from the comparison of the IR and hard X-ray emissions of Seyfert galaxies.

The X-ray spectral properties of the ‘hidden’ AGN are also relevant to the problem of the origin of the of the X-ray background (XRB). Setti & Woltjer (1989) first suggested that highly absorbed AGN (possibly Seyfert 2’s) may account for a major fraction of the XRB in the 3–30 keV range. This suggestion has been recently explored by Comastri et al. (1995) and Madau, Ghisellini & Fabian (1994) in the framework of the Seyfert’s unified scheme. However, some basic ingredients to compute the absorbed AGN contribution to the XRB, such as their total number and their hard local X-ray Luminosity Function (XLF), are still quite uncertain. No more than a dozen type-2 AGN have been detected by the HEAO-1 A1 all-sky survey (2–10 keV) and only a very tentative XLF has been derived (Grossan 1992). Extremely relevant information resides in the local X-ray volume emissivity (LXVE, i.e., the total amount of X-rays produced per unit volume in the nearby Universe), an integrated quantity which can be more easily constrained than a detailed XLF. The contribution of any class of source to the cosmic X-Ray Background (XRB) is indeed modulated by its LXVE and cosmic evolution (see for a review Fabian & Barcons 1992).

With the aim of probing the unified models and of estimating the contribution to the LXVE and to the XRB by low luminosity and ‘hidden’ active nuclei, we analyze with some detail in this paper the X-ray emission from a complete sample of AGN and galaxies selected at  $12\mu\text{m}$  by Rush, Malkan & Spinoglio (1993; henceforth RMS) and the IR emission of the largest available hard X-ray flux limited AGN sample (Grossan 1992). The latter is suitable to explore the ratio of the X-ray to IR luminosities of the AGN because it includes objects in a wide interval of luminosity (about 5 orders of magnitude). As for the RMS galaxy sample, the advantage of the  $12\mu\text{m}$  selection is in the large fraction of AGN, which amounts to  $\approx 13\%$  (to be compared with a typical  $\sim 1\%$  of optically selected or  $60\mu\text{m}$ -selected galaxy samples) and in the fact that it is not as biased against low luminosity and ‘hidden’ AGN as X-ray ( $< 10$  keV) selected samples: galaxy emission is in general at a minimum in the 5 to 25  $\mu\text{m}$  window, where ‘hidden’ AGN are expected to emit a significant fraction of their luminosity.

We study the LXVE of the RMS sample objects in the 2 – 10 keV band. Although the XRB intensity is unambiguously measured in this energy band (free from galactic contamination at high galactic latitudes, Marshall et al 1980) and all-sky maps are available (as given by the HEAO-1 A2 experiment), the origin of a large fraction of it ( $\gtrsim 75\%$ ) remains speculative. Exploitation of the rich sample of AGN in the RMS catalogue allows the determination of X-ray emissivities from active and non-active galaxies separately and the exploration of the emissivity of possible ‘hidden’ AGN. This is crucial to constrain models of the origin of the XRB based on the unified Seyfert scheme.

Various methods have been used to infer or measure the local X-ray volume emissivity of different classes of sources. The most obvious one is to directly search for X-ray emission around the positions of a given sample of sources. This was first tried by De Zotti et al. (1989) by searching in the A2 X-ray maps for emission of a list of galaxies emitting at  $12\mu\text{m}$  (actually a subsample of the RMS sample used in this paper). Although the large beam-aperture of the A2 collimator ( $3^\circ \times 1.5^\circ$ ) produced serious confusion problems, these authors were able to detect and quantify the emissivity from the Seyfert galaxies in their sample. But probably the currently most popular approach is to cross correlate complete galaxy catalogues with X-ray maps covering large enough regions (Jahoda et al. 1991, 1992; Lahav et al. 1993; Miyaji et al. 1994; Carrera et al. 1994). The method consists in smearing a usually large and complete galaxy catalogue (selected at some optical or far-infrared wavelength) with the same beam of the all-sky X-ray survey. A cross correlation between the beam-smearred galaxy catalogue and the X-ray map is expected to produce a positive signal if the catalogued galaxies have X-ray emitters associated with them.

We fully exploit in this paper the whole X-ray database of the HEAO-1 mission, including the A1 and A2 experiments. Although various other space observatories have surveyed at X-ray energies up to 10 keV or slightly above at fainter fluxes, HEAO-1 is currently, and will be for some time, the only one providing spectral sensitivity well above 10 keV (and up to  $\sim 60$  keV) over the entire sky. We judged that a detailed investigation based on such data would have provided unique information about that numerous class of

hard X-ray emitters predicted by the unified picture of AGN activity.

The paper is organised as follows. In Section 2 the data used is presented. It includes the RMS galaxy catalogue and its various subsamples, the hard X-ray flux-limited AGN sample by Grossan (1992), and finally the hard X-ray all-sky maps from the HEAO-1 A2 survey. In Section 3 we discuss the methods used to investigate the hard X-ray emissivity of various IR samples, including an Intensity Distribution Analysis (IDA) method (which generalizes the study by De Zotti et al 1989) and the CCF method which is also briefly outlined here and specifically tailored to our purposes. The results of the application of these methods are presented in Section 4. They concern the derivation of the average X-ray to  $12\mu\text{m}$  luminosity ratios and the XLF's for the various  $12\mu\text{m}$  galaxy samples, and estimates of the X-ray volume emissivities. Particular emphasis is given to Seyfert 1 galaxies, whose X-ray emission properties (in addition to the IR ones) are particularly well known. Discussions involving the existence of 'hidden' classes of AGN (i.e., optically classified as non-active), and constraints on the unified AGN model and implications on the synthesis of the XRB are given in Section 5. Conclusions appear in Section 6.

A Hubble constant  $H_0 = 50 \text{ km s}^{-1} \text{ Mpc}^{-1}$  and a deceleration parameter  $q_0=0.5$  are assumed.

## 2. THE DATA

### *2.1 The IRAS $12\mu\text{m}$ galaxy sample*

The RMS catalogue is a list of 835 high galactic latitude ( $|b| > 25^\circ$ ) extragalactic sources with *IRAS*  $12\mu\text{m}$  flux  $f_{12} > 0.2 \text{ Jy}$ , which is almost completely identified (more than 98%). For each source,  $\alpha$ ,  $\delta$ , the redshift and the fluxes in the 4 *IRAS* bands (12, 25, 60,  $100 \mu\text{m}$ ) are given. The sources are classified into 5 different categories: Seyfert 1 galaxies and QSOs, Seyfert 2 galaxies, Liners, Starburst galaxies (non-Seyferts with high FIR luminosity) and normal galaxies. Usual tests ( $V/V_{max}$  and log N-log S) show that both the whole sample and the various sub-samples are complete. Only the Seyfert 1 sample shows a marginal incompleteness, which Rush, Malkan and Spinoglio (1993) attribute to



the fact that some still unidentified Seyfert 1s could fall in the non-Seyfert samples.

Following previous studies exploiting *IRAS* colours of galaxies to identify IR-selected samples of AGN (de Grijp et al 1985), we have searched for unidentified AGN in the RMS sample through a multicolor analysis of *IRAS* data. We plot in Figure 1 the  $f_{12}/f_{100}$  vs  $f_{25}/f_{100}$  colour-colour diagram for various galaxy classes in the RMS sample.

We see that Seyfert galaxies occupy a well-defined elongated region on this plot, whereas that most of the non-Seyfert galaxies cluster around a different position in the graph. There are, however, a number of galaxies with FIR colours deviating from the average galaxian colour and spread over the AGN zone. These have a relatively larger  $12\mu\text{m}$  flux compared with the average galaxy, which implies a higher fraction of hot dust emission. According to our view (see also Danese et al, in preparation) these sources are prime candidates to host a hidden AGN. We have defined an IR sample of AGN candidates by selecting sources with  $f_{12}/f_{100} < 4000 (f_{25}/f_{100})^2$ , a criterion which maximizes the segregation between Seyfert and non-Seyfert galaxies in the colour plane of Fig. 1. These objects will constitute our Hot Dust Galaxy (HDG) sample.

To summarize, we have considered in this paper 5  $12\mu\text{m}$ -selected galaxy samples: Seyfert 1, Seyfert 2, normal galaxies (liners and starbursts are also included here given their small numbers in the RMS sample), Hot Dust Galaxies and the whole sample. We have excluded from our analysis  $10^\circ$  circles around Virgo ( $\alpha = 12^{\text{h}} 28^{\text{m}}$ ,  $\delta = 12^\circ 40'$ ) and the Large Magellanic Cloud ( $\alpha = 5^{\text{h}} 24^{\text{m}}$ ,  $\delta = -69^\circ 45'$ ). Table 1 (which also includes the results from our X-ray intensity distribution analysis) shows the number of objects contained in each subsample.

## 2.2 The X-ray data: the HEAO-1 A1 AGN sample

This paper is devoted to an assessment of the X-ray properties of mid-IR selected extragalactic sources. If one assumes that the hot dust responsible for the  $12\mu\text{m}$  emission is mostly heated by the central engine in AGN, then a roughly proportional relation is expected between the X-ray flux ( $f_X$ ) and the  $12\mu\text{m}$  flux. In order to test this hypothesis, we have considered the AGN sample (mostly Seyfert 1 galaxies) studied by Grossan (1992)

and including *IRAS* 12 $\mu$ m data. The sample has been derived from the HEAO-1 Large Area Sky Survey sample in the 2-20 keV band (Wood et al., 1984). The 12 $\mu$ m data are from an add-scan (SCANPI) analysis of the *IRAS* survey.

More than 86% of the sources have been identified above a flux limit of 0.95  $\mu$ Jy at 5 keV. Ninety six emission line AGN (85 Seyfert 1 and QSOs and 11 Seyfert 2 galaxies) make up the complete X-ray sample. As shown by Turner & Pounds (1989) and by Nandra & Pounds (1994) and also implied by spectral information on the Piccinotti et al (1992) AGN sample, classified Seyfert 1 galaxies are characterized by values of the column density  $N_{HI}$  of absorbing material typically lower than  $10^{22}$  cm $^{-2}$ , whereas type-2 objects have almost invariably larger amounts of gas.

A plot of the monochromatic 5 keV and 12 $\mu$ m luminosities (including IR detections and upper limits) is shown in Figure 2. We can see there an approximately linear relation, which however appears to break down at both low and high luminosities. At  $L_{12} < 10^{30}$  erg s $^{-1}$  Hz $^{-1}$  ( $L_{12}$  denotes the luminosity at 12 $\mu$ m) the IR flux is probably dominated by the contribution from diffuse dust in the host galaxy, and this flattens up the relationship between IR and X-ray luminosities. On the contrary, a break down at the high luminosities may be qualitatively inferred from the fact that over 40% of the objects with 5 keV luminosity  $L_X > 10^{26}$  erg s $^{-1}$  Hz $^{-1}$  and virtually all but three radio-loud AGN at  $L_X > 10^{27}$  erg s $^{-1}$  Hz $^{-1}$  have no *IRAS* detection at 12 $\mu$ m (above an average flux limit of  $f_{12} \simeq 0.1$ Jy), whereas for the whole sample the IR detection rate approaches 80%. This is not due to a flux selection artifact, since excluding the 14 brightest Seyfert 1s in Grossan's sample (which have fluxes above 2 $\mu$ Jy@5 keV) the remaining sources exhibit a uniform distribution in X-ray flux of the fraction of undetections to detections at 12 $\mu$ m down to the limiting X-ray flux.

A detailed, more quantitative discussion of these effects and possible interpretations will be given in Sections 4 and 5 below.

### 2.3 The X-ray data: the HEAO-1 A2 database

The database used to estimate the X-ray emissivity of the various RMS samples consists of

the HEAO-1 A2 all-sky survey map constructed with the MED and the HED # 3 (the A2 *total* band). Although this broad band has sensitivity from 2 to 60 keV, we formally keep using the 2-10 keV range as our reference band. We have also made use of the A2 *hard* band data sensitive to photons in the 6-60 keV energy range (Allen, Jahoda & Whitlock 1994).

Since confusion is the most severe problem in our analysis, we choose to keep only the  $3^\circ \times 1.5^\circ$  collimators, for which the conversion factor is  $2.1 \times 10^{-11}$  erg cm $^{-2}$  s $^{-1}$  per R15 count s $^{-1}$  for a power-law spectrum with energy index  $\alpha_X = 0.7$ . The shape of the collimator is assumed to be triangular in both axes with FWZI of  $6^\circ \times 3^\circ$  (which is  $3^\circ \times 1.5^\circ$  FWHM):

$$G(\vec{x}) = \text{Max} \left( 0, 1 - \frac{|x|}{3^\circ} \right) \text{Max} \left( 0, 1 - \frac{|y|}{1.5^\circ} \right) \quad (1)$$

The all sky map is in the form of a  $720 \times 720$  matrix in ecliptic coordinates. Measurements are separated  $0.5^\circ$  in ecliptic longitude and  $0.25^\circ$  in ecliptic latitude, therefore providing a set of highly overlapped measurements of the X-ray sky intensity. These datapoints are strongly dependent, but they provide a fine enough grid for our purposes.

### 3. THE METHODS

#### *3.1 The X-ray Intensity Distribution Analysis (IDA) around IR source positions*

Roughly speaking this method consists in the measurement of the X-ray intensity in the positions of the sources, and a comparison of this intensity histogram against some reference or ‘blank sky’ distribution. If there is a significant difference (that we will test with the one sided Kolmogorov-Smirnov statistic) we would have then detected a signal of X-ray emission from the source sample. We will then model this difference in terms of either a constant  $f_X/f_{12}$  ratio or of a  $f_X$ -to- $f_{12}$  non-linear parametric relation. This method (already used by De Zotti et al. 1989) has the advantage over an all-sky CCF in that it does not use data from points where there are no sources. This is especially relevant to our case, since the total sample has only about 0.1 sources per beam and so 9 out of 10 X-ray data measurements only introduce noise in the CCF.

The IDA method, however, has some subtleties that can only be properly met by numerical simulation techniques. Both the significance of any putative signal and the determination of the relation between  $L_X$  and  $L_{12}$  have been done by making simulations of the X-ray sky and then performing measurements of the X-ray intensity distribution around the positions of the sources exactly in the same way as in the real sky. To generate a ‘blank sky’, we have first measured the X-ray intensity collected by the collimator in a large number of positions at  $|b| > 25^\circ$  and excluding the Virgo and LMC regions. This is used as the parent distribution from which we draw a ‘blank sky’ map. Each one of the  $720 \times 720$  sky elements is replaced by a random measurement of the above list. It is clear that this does not reproduce the positional structure of the real sky, neighbouring X-ray intensities being no longer correlated. However, this simple algorithm does not bias the one-point background intensity distribution in any way.

The next step is to add the sources of the corresponding subsample. This is done by beam-smearing (according to eq. 1) the source sample under consideration, assigning a given relation between  $f_X$  and  $f_{12}$ . In that synthetic sky map, we perform the same measurement as in the real sky X-ray map, i.e., we build a histogram with the intensities associated to the source positions. These intensities are obtained, both when measuring on the real X-ray sky and on the synthetic sky, by a bilinear interpolation of the 4 nearest measurements. Although this effectively sharpens the histograms (a bilinear interpolation acts as a smoothing procedure), the method is correct as long as the same type of measurement is performed to the data and to the simulations.

The resulting histograms are compared via the one-sided Kolmogorov-Smirnov test. A number of simulations (typically 10) are performed for each tested X-IR relationship. We find that the KS statistic from the comparison of these simulations with the real data has usually little scatter and therefore 10 simulations have been found to be enough. Our best fits always provide a good enough description of the data, the rejection probability being  $< 50\%$ . All quoted errors and upper limits refer to the 95% confidence level.

For Seyfert 1 galaxies not only the X-ray signal is stronger, but also a complementary

information from X-ray selected samples can be used. In this case we have also tested more general non-linear regressions of the X-ray on the IR flux (see details in Sect.4):

$$\log L_X = a + b \log L_{12}, \quad (2)$$

$L_X$  and  $L_{12}$  being the monochromatic luminosities in  $\text{erg s}^{-1} \text{Hz}^{-1}$  at 5 keV and at  $12\mu\text{m}$ , respectively. In addition to this simple one-to-one relation, we have also tested regressions with gaussian distributions of the residuals.

We emphasize that this technique properly accounts for the most severe problem that we have in this analysis, i.e. the source confusion in the A2 beam. Since the measurements are performed exactly in the same way in the real and simulated sky, there is no double counting effect for those cases where two  $12\mu\text{m}$  sources fall within a beamsize, no matter whether or not sources are clustered. This procedure does not account for the part of the clustering effect where one or more clustered X-ray sources, which are not themselves among the  $12\mu\text{m}$  sample, are within one beam of a  $12\mu\text{m}$  source. However, given the size of the beam, the estimated excess flux from the clustering effect is one order of magnitude smaller than the X-ray flux from the  $12\mu\text{m}$  sources themselves, for any reasonable values of the volume emissivity and clustering properties. Even though, this is quite difficult to reproduce in analytical terms. A further advantage of this method is that we are fitting a quantity (the X-ray to  $12\mu\text{m}$  luminosity or flux relation) which has a direct physical meaning and requires no further hypotheses to be translated into, e.g., the LXVE.

### 3.2 The Cross-Correlation Function (CCF)

We use here the zero-lag cross correlation function between the beam smeared version of the samples introduced in Section 2.1 and the map of the X-ray sky presented in Section 2.3. It is defined as

$$W = \frac{\langle N_B I_B \rangle}{\langle N_B \rangle \langle I_B \rangle} - 1 \quad (3)$$

where  $N_B$  is the number of sources per beam and  $I_B$  the X-ray intensity per beam. Averages are taken over all available beams restricted to  $|b| > 25^\circ$  and avoiding the Virgo and

LMC regions.

The interpretation of the CCF in terms of the local volume emissivity has been presented in several papers (Jahoda et al. 1992; Lahav et al. 1993; Miyaji et al. 1994; Carrera et al. 1994). Defining  $\eta = W\langle N_B \rangle \langle I_B \rangle$ , there are two contributions expected to this number - a Poisson contribution ( $\eta_P$ , due to the coincidence of having an X-ray source associated with a catalogued source) and a contribution from source clustering ( $\eta_{cl}$ , this is to account for the fact that the source number density is enhanced around the catalogued sources). Following the above works we can write these contributions as

$$\eta = \eta_P + \eta_{cl} = \frac{1}{4\pi} j_0 \omega_{col}(0) (R_P + R_{cl}) \quad (4)$$

where  $j_0$  is the LXVE due to the catalogued sources,  $R_P$  and  $R_{cl}$  have dimensions of a length and reflect the contributions of the Poisson and clustering terms respectively and  $\omega_{col}(\vec{x})$  is the collimator correlation function defined as

$$\omega_{col}(\vec{x}) = \int d^2x' G(\vec{x}') G(\vec{x}' - \vec{x}) \quad (5)$$

and  $G$  is the beam triangle function of eq. (1).

The poisson depth  $R_P$  is just the X-ray depth of the catalogue

$$R_P = \int dR P_x(R) \quad (6)$$

where  $P_x(R)$  is the X-ray selection function. To be consistent with the study performed in Section 3.1, we compute this selection function in terms of the  $12\mu\text{m}$  luminosity function. The selection function is therefore (see eq (4) in Miyaji et al. 1994)

$$P_X(R) = \frac{\int_{4\pi R^2 f_{lim}}^{\infty} dL_{12} L_X(L_{12}) \Phi_{12}(L_{12})}{\int_0^{\infty} dL_{12} L_X(L_{12}) \Phi_{12}(L_{12})} \quad (7)$$

where  $f_{lim} = 0.2$  Jy is the limiting flux of the  $12\mu\text{m}$  sample and  $\Phi_{12}(L_{12})$  the corresponding luminosity function.

Assuming that the source correlation function can be parametrized as a power law

$$\xi(r) = \left( \frac{r}{r_0} \right)^{-\gamma} \quad (8)$$

(values  $r_0 = 8 h_{50}^{-1}$  and  $\gamma = 1.65$  will be used throughout as representative of IR selected galaxies, although there is some uncertainty here), the clustering depth can be written as

$$R_{cl} = \langle n \rangle H_\gamma A_\gamma r_0^\gamma \int d^2x \frac{\omega_{col}(\vec{x})}{\omega_{col}(0)} |\vec{x}|^{\frac{1-\gamma}{2}} \quad (9)$$

where  $H_\gamma = \Gamma(1/2)\Gamma((\gamma-1)/2)/\Gamma(\gamma/2)$ ,  $\langle n \rangle$  is the average source density per unit volume and

$$A_\gamma = \int dR R^{3-\gamma} P_{12}(R) \quad (10)$$

where the  $12\mu\text{m}$  selection function is

$$P_{12}(R) = \frac{\int_{4\pi R^2 f_{lim}}^\infty dL_{12} \Phi_{12}(L_{12})}{\int_0^\infty dL_{12} \Phi_{12}(L_{12})} \quad (11)$$

The average source density can be easily estimated from this function by noting that

$$\langle N_B \rangle = \Omega_B \langle n \rangle \int dR R^2 P_{12}(R) \quad (12)$$

where  $\Omega_B = \int d^2x G(\vec{x})$  is the effective beam solid angle.

The selection functions (and consequently the depths  $R_P$  and  $R_{cl}$ ) can be easily estimated when the catalogue is large. As we shall see later, this is not quite the case in our catalogues, especially for the shortest subsamples. The errors in these quantities will in fact propagate to large errors in the estimate of the LXVE which is given by

$$j_0 = \frac{4\pi W \langle N_B \rangle \langle I_B \rangle}{\omega_{col}(0)(R_p + R_{cl})} \quad (13)$$

## 4. RESULTS

### 4.1 X-ray signals for various IR galaxy populations and the average $f_X/f_{12}$ flux ratios

Table 1 shows the results of the application of the IDA method (see Sect. 3.1) to the 5 RMS subsamples (Sect. 2.1) where we have assumed a constant  $f_X/f_{12}$  flux ratio for each subsample. Figure 3 shows the comparison between the ‘blank sky’ intensity histograms and the measured ones for the 5 samples defined in Section 2.1.

A visual inspection of Fig. 3 evidentiates that Seyfert 1 galaxies produce a large and highly significant signal, also confirmed by the KS test. The  $f_X/f_{12}$  value found is entirely consistent with the one previously obtained by De Zotti et al. (1989). Seyfert 2s also produce a detectable effect (at a  $> 2\sigma$  level), but their X-ray to  $12\mu\text{m}$  flux ratio is  $\sim 7$  times smaller than for Seyfert 1s. If Seyfert 2 galaxies are just obscured Seyfert 1 galaxies, at high enough energies (where photoelectric absorption and Compton scattering would be negligible) both of them should have similar flux ratios. In the unified scheme the obscuring tori are expected to be Compton thick and therefore X-rays will only escape in the Klein-Nishina regime, i.e., at energies above several tens of keV, which are only marginally accessible to the A2 detectors. Keeping that in mind we examined the histograms in the hard band (corresponding to energies  $> 10$  keV), but they are too noisy (too broad) to test for the differences with the total band case (see Fig 4). Indeed, based upon the high-energy channels of the X-ray maps, we find for Seyfert 1 galaxies  $f_X/f_{12} = (1.4_{-0.8}^{+1.0}) \times 10^{-6}$  and for Seyfert 2 galaxies  $f_X/f_{12} = (0.3_{-0.3}^{+0.4}) \times 10^{-6}$ , i.e. consistent with the results from the total band but with larger errors and also not too far from Seyfert 1 and 2 having similar flux ratios.

On the other hand we do not find any significant signal coming from the galaxy (non-Seyfert) sample. The upper limit found shows that in terms of  $f_X/f_{12}$  the average normal galaxy is more than  $\sim 20$  times fainter than a Seyfert 1 and more than  $\sim 2$  times fainter than the average Seyfert 2 galaxy.

However, it might still be possible that a fraction of these galaxies do produce some X-rays, but their signal is diluted throughout the sample. That would be the case if, for example, some Seyfert 1s were misidentified as galaxies. If we assume that these objects have a X-ray to  $12\mu\text{m}$  flux ratio typical of Seyfert 1s, they could be at most  $\sim 6\%$  of the galaxy sample, which is still 41 objects (i.e. a number comparable to that of the RMS Seyfert 1 sample).

Since it is likely that these X-ray emitters in the galaxy sample have FIR colours similar to AGN, some signal would be expected from the Hot Dust Galaxy sample. Table



1 shows that there is no such signal and that the 95% upper limit for the X-ray to  $12\mu\text{m}$  flux ratio is rather small. If all of the type 1 active objects missed would be included in this hot far-IR sample, we can conclude that less than 7% (i.e., less than 11 objects) of the Hot Dust Galaxies can be Seyfert 1s. This poses an upper limit of 20% to the number of unrecognized Seyfert 1 galaxies.

We have also carried out the analysis for the whole sample, irrespective of classification. A signal is also detected at a significance  $> 95\%$  in this case, with an average X-ray to  $12\mu\text{m}$  flux ratio of  $0.8 \times 10^{-7}$ , most of which comes indeed from the active objects.

All these results are confirmed and strengthened by the CCF analysis. Such results for the different sub-samples are shown in Table 2. The errors on the CCF (always 95% confidence errors) are drawn from simulations of randomly placed sources according to the source density for each case, since bootstrap reshuffling of the list of  $(N_B, I_B)$  pairs results in a significant underestimate of the errors. It can be immediately seen that normal galaxies and the Hot Dust Galaxies do not produce any significant signal in the CCF as in the IDA approach. A signal from the Seyfert 1 and Seyfert 2 galaxies is detected, although the signal from the whole sample is no longer significant. This last fact has to be understood in terms of a large chance probability of having sources coincident with high-intensity X-ray spots when the number of sources is large enough.

#### *4.2 The relationship between X-ray and mid-IR emission for Seyfert galaxies*

As anticipated, for Seyfert 1 galaxies we are in the position to perform quite a detailed comparison of hard X-ray and IR properties, by exploiting both the A2 survey information on *IRAS*-selected objects and the  $12\mu\text{m}$  *IRAS* survey data for the A1 AGN sample (Sect. 2.2). For both selections we have complete samples with redshift information, so that we can easily build up local luminosity functions (LF) and bivariate luminosity distributions. The IR luminosity functions for the various RMS samples have been derived by Rush et al. (1993, see Figure 6 below). The simplest way to estimate a local XLF for Seyfert 1 galaxies starting from the  $12\mu\text{m}$  function would be to transform it through the average  $f_X/f_{12}$  flux ratio reported in Table 1, then assuming that this factor does not depend on the luminosity

and that any intrinsic scatter around this mean value is negligible. A comparison of such a local XLF with those derived by Piccinotti et al (1982) and Grossan (1992) (see Figure 5) shows that the two roughly agree at low luminosities, but at medium-to-high  $L_X$  the predicted XLF based on the IR selection keeps significantly below the observed one.

A similar exercise of predicting a LF at  $12\mu\text{m}$  for Seyfert 1s, starting from the observed XLF, can be done using an average regression of  $L_{12}$  vs.  $L_X$ . We have fitted an average regression to the  $L_X$ - $L_{12}$  data on Seyfert 1s which appear in Figure 2. Such an operation brings to an IR LF which also keeps below on average, and particularly at medium-to-low luminosities, with respect to that estimated by Rush et al (see Figure 6).

To overcome the above inconsistencies, we have taken into account the effects of an intrinsic (i.e. not due to observational errors) dispersion of the residuals in the  $L_X$ - $L_{12}$  ratio. An obvious consequence of this dispersion is to rise the predicted LF, as discussed for example in Franceschini et al. (1994). Taking this into account brings to a better match of the X-ray LF's, but worsens the fit of the IR ones at the high luminosities, where the values predicted starting from the A1 XLF now exceed significantly the observations.

The only way we found to bring all these observables into agreement was to assume a non-linear average scaling of  $L_X$  on  $L_{12}$ , as parametrized in eq.(2) and with  $b > 1$ , and to assume an appreciable dispersion  $\sigma(\log[L_X/L_{12}])$  of the residuals around this average regression.

There are five parameters in this model: the normalization  $a$  and slope  $b$  in eq.(2) and the dispersion  $\sigma(\log[L_X/L_{12}])_{IR}$  for the IR-selected AGN, the normalization  $a'$  and  $\sigma(\log[L_X/L_{12}])_X$  of the average regression line for the X-ray selected AGN. We have obviously assumed that both the slope  $b$  and the intrinsic dispersion  $\sigma(\log[L_X/L_{12}])$  keep roughly the same values for the two selections (see Cheng et al., 1984). To derive best-fit values of  $a$  and  $b$  for the RMS Seyfert 1s, given a value for  $\sigma(\log[L_X/L_{12}])$ , we have performed a set of simulations as explained in Sect. 3.1 and compared with the A2 survey intensity distributions. We report in Table 3 a set of results for  $a$  and  $b$ , assuming  $\sigma(\log[L_X/L_{12}]) = 0.5$ , which is derived from the rms deviations to the fit shown in Fig. 2.

Cheng et al. (1984) have shown that in the case of a linear dependence ( $b = 1$ ) and for local objects, there is a simple relation between the average luminosity ratios for the two selections and the dispersion of residuals:

$$\langle \log(L_{12}/L_X) \rangle_{IR} = \langle \log(L_{12}/L_X) \rangle_X + \frac{3}{2} \ln(10) \sigma^2(\log[L_{12}/L_X]), \quad (14)$$

where  $\sigma$  is the same for both selections. This implies a link between the parameters  $a$ ,  $a'$  and  $\sigma$ . Eq.(14) is only slightly modified in the case that  $b \neq 1$ . In such a case the two dispersions  $\sigma$  do not coincide, being related by

$$\sigma(\log[L_X/L_{12}])_{IR} = b \sigma(\log[L_X/L_{12}])_X, \quad (15)$$

where the left-hand quantity is the dispersion of the conditioned probability distribution of the residuals for a given  $L_{IR}$  and for IR-selected objects, and viceversa for the right-hand quantity.

The best-fit parameter values able to reconcile the IR and X-ray LF's are  $a = -15.25$ ,  $b = 1.3$ ,  $\sigma(\log[L_X/L_{12}])_{IR} = 0.51$ ,  $a' = -14.36$ . From these values and eq.(15) we infer  $\sigma(\log[L_X/L_{12}])_X \simeq 0.4$ . An important counter-check is to compare the normalizations  $a$  and  $a'$  with eq.(14):  $a' = a + 0.897 \simeq -14.35$ , indeed quite consistent with our previous values. So we are confident that our description of the IR-X relationship is accurate enough.

Figures 5, 6 and 2 report the model predictions versus observations for the hard X-ray (2-10 keV) and  $12\mu\text{m}$  LF's, and for the  $L_X - L_{12}$  plot. Particularly relevant for us, by means of a  $\chi^2$ -test comparison of predicted and observed LF's in the X-rays and IR, we estimate 95% confidence limits on the average slope  $b = 1.3_{-0.05}^{+0.1}$ : this means a very significant non linearity of the average  $L_X$ - $L_{12}$  regression, in the sense that at the higher IR luminosities the X-to-IR flux ratio becomes higher and higher. This non-linear behaviour is not only suggested by a direct inspection of the observed  $12\mu\text{m}$  fluxes of hard X-ray AGN (Fig.2), but also more strongly required to reconcile the observed LF's of Seyfert 1 galaxies in the IR and X-rays.

The much fainter X-ray signals provided by the IDA or CCF analyses for Seyfert 2s galaxies do not warrant the same detailed investigation being performed for type-1 objects.

A comparison of the rough 2-10 keV XLF based on the small Seyfert 2 A1 sample (Sect. 2.2) with predictions based on the IR LF and on the average observed flux ratio shows that in this case too a sizeable scatter of the residuals plays an important role. Matching the observed  $\langle \log(L_X/L_{12}) \rangle$  for IR- and X-ray selected objects (which differ by roughly a factor of ten in this case) implies a value  $\sigma[\log(L_X/L_{12})] \gtrsim 0.55$ , slightly higher than that of type-1 AGN. The dot-dashed line in Fig. 5 corresponds to a prediction for Seyfert 2s based on the IR LF, a constant flux ratio (as in Table 1), and this residual distribution. We see it consistent with the A1 XLF, within the large statistical uncertainties.

#### *4.3 Constraints on the local X-ray volume emissivities*

Figure 5 compares the observed 2-10 keV XLF's with inferences based on IR selected samples of galaxies and AGN. The thick lines correspond to the predicted contribution of Seyfert 1s and 2s, as discussed in detail in the previous section. For the non-Seyfert galaxies only an upper limit can be set which is also represented as thin continuous lines.

Inspection of Fig 5 reveals that the XLF is by far dominated over most of the luminosity range by Seyfert 1 galaxies, type 2 objects contributing only at the lowest luminosities. This agrees with the identification rates of the two types in the A1 AGN sample (only 8 Seyfert 2 over 96 objects).

So, the situation is rather clear in the  $10^{42} - 10^{46} \text{ erg s}^{-1}$  X-ray luminosity range, where most (if not all) the XLF is accounted for by Seyfert (mostly type 1) galaxies emitting at  $12\mu\text{m}$ . Below  $10^{42} \text{ erg s}^{-1}$  the situation is still unclear. The number densities of Seyfert 1 and Seyfert 2 galaxies become similar, but the non-Seyfert galaxies might in fact start to dominate. If the contribution of the non Seyferts is close to their 95% upper limit, the XLF will continue rising below  $10^{42} \text{ erg s}^{-1}$ . However, as emphasized many times, we do not detect any X-ray signal from these objects, and therefore this has to be strictly taken as an upper limit.

With the use of these XLFs for the different classes of objects, their contribution to the LXVE can be found. The results are listed in the last entry of table 1. The LXVE is clearly dominated by the Seyfert 1 galaxies and only some small extra contribution arises

from the Seyfert 2s. The contribution of these separate classes is more precisely found than the total contribution by analysing the whole sample irrespective of the classification. This shows the importance of isolating the classes that produce and do not produce X-rays as we have done here. Note that all quoted values of LXVE in Table 1 (and Table 2 below) are *equivalent* emissivities in the 2-10 keV band, i.e. they are the fluxes in that waveband corresponding to sources providing the observed signal in the A2 maps and having power-law spectra with energy slope  $\alpha_X = 0.7$ . This means that the reported values of LXVE take into account in detail of the A2 response function allover the 2-60 keV band.

The CCF analysis provides an alternative method to estimate the LXVE. To extract it from the measurements of the CCF (Table 2) we have to estimate the depths  $R_P$  and  $R_{cl}$  from the catalogues themselves. Using eq. (6) and assuming  $L_X \propto L_{12}$  the Poisson depth can be obtained as

$$R_P = \frac{\mathcal{N}}{\sum_{i=1}^{\mathcal{N}} \left( \frac{L_i}{4\pi f_{lim}} \right)^{-0.5}} \quad (16)$$

where for simplicity  $L_i$  denotes the  $12\mu\text{m}$  luminosity of the  $i$ -th source in the catalogue (which totals  $\mathcal{N}$  sources and the sums are performed over the whole catalogue). We can similarly estimate the parameters  $A_\gamma$  and  $\langle n \rangle$  as

$$A_\gamma = \frac{1}{4 - \gamma} \frac{\sum_{i=1}^{\mathcal{N}} \left( \frac{L_i}{4\pi f_{lim}} \right)^{\frac{1-\gamma}{2}}}{\sum_{i=1}^{\mathcal{N}} \left( \frac{L_i}{4\pi f_{lim}} \right)^{-\frac{3}{2}}} \quad (17)$$

$$\langle n \rangle = \frac{3\langle N_B \rangle}{\Omega_B} \sum_{i=1}^{\mathcal{N}} \left( \frac{L_i}{4\pi f_{lim}} \right)^{-\frac{3}{2}}. \quad (18)$$

Since our catalogue lists are rather short, these numbers are subject to significant uncertainties. In order to estimate them, we bootstrapped the catalogue, measured these quantities and computed  $R_P$  and  $R_{cl}$ . The 95% errors are also shown in Table 2 where it can be seen that these errors are rather large. Another interesting feature to realize is that the clustering depth  $R_{cl}$  is always smaller than the Poisson depth  $R_P$ , as opposed to the samples studied in Lahav et al. (1993), Miyaji et al. (1994) and Carrera et al. (1995). The

reason is simply that our samples are so sparse that the probability of having two sources in the same beam for a given source correlation function is small even for the whole sample (see source density entry in Table 2).

The resulting LXVE from the CCF for the different subsamples is shown in last entry of Table 2. We can see that the uncertainties introduced by the errors in the catalogue depths translate to sizeable variations in this number. Comparing the last column of Tables 1 and 2 we see that the LXVE estimates obtained by the CCF method are consistent with those obtained via the intensity distribution method.

However some differences in the results of the two approaches must be noticed. Since the CCF method assumes constant  $L_X/L_{12}$  ratio, its prediction on the LVXE of the Seyfert 1 galaxies is in agreement with the value derived by using the IDA method under the same assumption. The IDA technique is more flexible, as it allows to test more complex relationships between IR and X-ray luminosities. On the other hand this method makes use of a much noisy synthetic ‘blank sky’ and as a consequence it soon impingies on the background noise when the analysis concerns classes of intrinsically faint objects. This is demonstrated by the relatively loose upper limits to the LXVE of the HDG and normal galaxy classes derived with the IDA method. Thus this method is effective in studies of populations with significant emission.

Conversely, the CCF method provides a more integrated information, but has a lower intrinsic noise, particularly when the sample size is large enough (galaxies and HDG’s). Moreover, contrary to the IDA, it makes full use of the topological information present in both the X-ray sky maps and the source spatial distribution. It is then more effective in setting tighter limits to the emissivity of classes of weakly emitting objects. This is particularly true when the source population under test has a spatial distribution uncorrelated with the main sources of the X-ray background flux. In our case, a CCF applied to non-active galaxies or HDG’s is weighted preferentially by sky regions where the X-ray background noise is lower than average.

Then the two methods appear to provide somewhat complementary information on

source emissivities.

## 5. DISCUSSION

### *5.1 Emission properties of AGN in the infrared and hard X-rays*

For Seyfert 1 galaxies, for which strong X-ray signals were found, our analysis has shown that the relation between X-ray and mid-IR emission is markedly non-linear: powerful X-ray sources are found to be relatively weak emitters at  $12\mu\text{m}$ . This evidence came not only by an inspection of directly measured fluxes in Fig. 2 (a direct but noisy and non-conclusive indication, because of the wide scatter on the  $L_X - L_{12}$  plane), but even more from a comparison of the IR and X-ray local luminosity functions, indirectly but very significantly requiring a non-linear scaling of the two emissions.

We have described such an effect in terms of a simple power-law regression, as in eq. (2). It is however quite possible that the real effect is that of an abrupt turn-off of the IR emission at the highest values of the underlying nuclear power which is traced by the hard X-ray flux. In addition to this, we also expect some contributions to the IR flux coming from the host galaxy, and appearing in the lowest luminosity objects. It is easy to verify, however, that the IR contribution of the host galaxy cannot explain by itself a non-linear behaviour for objects spanning a very large range of luminosities.

These observations impact on our understanding of the origin of the mid-IR emission in Seyfert 1 galaxies. Models of Seyfert 1 nuclei based on the assumption that the hard X-ray emission is produced by inverse Compton scattering on IR photons by relativistic electrons would predict a roughly linear relationship between X-ray and IR emission (see e.g. Band & Malkan 1989).

In the framework of unified schemes most of the mid-IR flux is expected to originate from the dust in the tori around the nuclei. In the simplest version of the scheme (for which only the orientation of the line of sight is relevant to the classification of the AGN) we expect that a quasi linear relation still holds, since dust is heated by nuclear UV radiation, which in turn is likely to be proportional to the hard X-ray luminosity. This is based on a recent analysis by Franceschini et al (1994) which shows that  $L_X \propto L_{opt}$  (and

consequently  $L_X \propto LUV$ ) as opposed to previous work by Avni & Tananbaum (1986) who found  $L_X \propto L_{opt}^{0.8}$ . In any case, the increase of the  $L_X/L_{IR}$  ratio with increasing  $L_X$  can be explained only if the torus covering factor is a decreasing function of the total nuclear power.

Some support to this hypothesis appears to follow from the comparison of the  $12\mu\text{m}$  and hard X-ray LFs of Seyfert 1 and 2 galaxies. It is apparent from figures 5 and 6 that luminous type 2 Seyferts are much rarer than luminous type 1 Seyferts both in X-ray (see Grossan 1992) and at  $12\mu\text{m}$ . While the result in the X-ray band can be possibly explained by an *ad hoc* assumption on the hydrogen column density, the  $12\mu\text{m}$  sample corroborates the conclusion that Seyfert 2 are intrinsically fainter than Seyfert 1 galaxies.

The difference of a factor of  $\sim 7$  in the average X-ray to IR flux ratios for type 1 and type 2 Seyferts (Table 1) has to be understood in terms of the obscuring material in Seyfert 2s being Compton thick, in which case virtually no X-rays escape below 10 keV. Indeed, the thick torus will be viewed quasi-equatorially for obscured objects, resulting also in a relative decrease of the Mid-IR emissivity with respect to Seyfert 1s, but still the ratio  $L_X/L_{12}$  is expected to drop substantially when going from face-on to edge-on viewing angles in this case. However, none of these facts can explain why  $L_{12}$  is suppressed for high luminosity AGN.

A difference of a factor of  $\sim 7$  in the average X-ray to IR flux ratios for type-1 and type-2 Seyferts (Table 1) might be explained, if all emissions are truly nuclear, only assuming that a column density as high as  $\sim 10^{25} \text{ cm}^{-2}$  covers type-2 objects. This implausibly high  $N_{HI}$  value appears to imply that a sizeable fraction of the mid-IR emission in Seyfert 2s is not of nuclear origin.

In conclusion we find evidences that the unified scheme must be complemented with the additional requirement that at increasing source power the covering factor of the torus significantly decreases, possibly due to the destruction of the torus by the radiation field. This is in keeping with the result claimed by Lawrence (1991) on the basis of the analysis of the relative number of narrow- and broad-line AGN in the 3CR catalogue.



## 5.2 The local X-ray volume emissivities

Our global estimates of the LXVE from sources emitting at  $12\mu\text{m}$ , based on the IDA method and the assumptions of a constant  $f_X/f_{12}$  flux ratio and negligible scatter of the residuals, are summarized in Table 1. For the two X-ray emitting classes, the Seyfert 1s and 2s, we know additional details about the bivariate  $L_X/L_{12}$  luminosity distributions. Taking them into account, the estimates of the corresponding LXVE change to  $j_X \simeq (4.0 \pm 1.5) \times 10^{38} h_{50} \text{ erg s}^{-1} \text{ Mpc}^{-3}$  (Seyfert 1s) and  $j_X \simeq (0.77^{+0.2}_{-0.5}) \times 10^{38} h_{50} \text{ erg s}^{-1} \text{ Mpc}^{-3}$  (Seyfert 2s, quoted errors always at  $2\sigma$ ). Those based on the CCF analysis are given in Table 2.

Altogether, our estimates of the LXVE are entirely consistent with those obtained by Miyaji et al. (1994) for the  $60\mu\text{m}$  2 Jy sample using the same X-ray data ( $(4.3 \pm 1.2) \times 10^{38} h_{50} \text{ erg s}^{-1} \text{ Mpc}^{-3}$ ). This is not a completely obvious result, since selection at  $60\mu\text{m}$  favours actively star forming galaxies (with little fractional content of AGN) while selection at  $12\mu\text{m}$  emphasizes the AGN content of the sample. Also, the Miyaji et al (1994) correlation analysis is dominated by clustering while our IDA and CCD are Poisson dominated.

Indeed we do not find evidence for X-ray emission coming from the non-Seyfert galaxy population (which should include the contribution of the starburst galaxies that dominate the  $60\mu\text{m}$  samples). The upper limits to the equivalent local volume emissivity for non-Seyfert galaxies (including liners and starbursts, as classified by Rush et al, 1993) is  $3.4 \times 10^{38} h_{50} \text{ erg s}^{-1} \text{ Mpc}^{-3}$  from the IDA and of  $1.0 \times 10^{38} h_{50} \text{ erg s}^{-1} \text{ Mpc}^{-3}$  from the CCF. For both the confidence is higher than 95%.

Our main conclusion is that the local volume emissivity is dominated by Seyfert 1 galaxies (and to a lesser extent by Seyfert 2). The fact that the RMS sample contains such a large fraction of AGN has allowed us for the first time to directly show that the LXVE is indeed due to a small fraction of galaxies rather than being distributed randomly over the whole galaxy population.

Should a fraction of the non-Seyfert galaxies contribute somewhere to the hard X-ray luminosity function (Fig. 5), that could happen only at quite low X-ray luminosities.

### *5.3 Hidden Active Galactic Nuclei and the fraction of covered to uncovered AGN*

It is instructive to see whether our analysis can set any interesting upper limit upon the number density of hidden AGN (i.e., objects classified as ‘normal’ galaxies but hosting a low luminosity active nucleus) on the basis of upper limits to the X-ray emission from non-Seyfert galaxies and even better from the Hot Dust Galaxies which should be prime candidates to host these hidden active nuclei.

Our upper limits imply that less than 20% of the total Seyfert 1 population are missed inside the Hot Dust Galaxy sample. We believe this to be a firm upper limit to the fraction of non-absorbed AGN which have been misidentified. However, these hidden AGN are more likely to have properties similar to Seyfert 2 galaxies. Taking the average X-ray to  $12\mu\text{m}$  flux ratio for the  $12\mu\text{m}$ -selected Seyfert 2s and the 95% upper limit on this ratio for the Hot Dust Galaxies we can conclude that at most 50% of these Hot Dust Galaxies might be misidentified Seyfert 2s. That means that at most 50% of the Seyfert 2 galaxies (always 95% upper limit) could have been misidentified as non-active galaxies if the X-ray to  $12\mu\text{m}$  flux ratio as the one measured here holds for these objects (see again Table 1). We can then conclude that at most 50% of the Seyfert 2 galaxies can be hidden. Since the space densities of type-1 and type-2 Seyferts in the RMS sample are comparable, this would imply that the global number of ‘covered’ AGN is less than a factor of two larger than that of the ‘uncovered’. This argument, however, assumes that hidden AGN have warm far-IR spectra and X- to  $12\mu\text{m}$  flux ratios similar to those of Seyfert 2s, and then is not conclusive about the question of the fractional importance of such population. In particular, if there is some sort of bias which has selected in our Seyfert 2 sample those objects which are Compton thin, as opposed to the hidden AGN which would be surrounded by Compton thick tori, our X-ray to  $12\mu\text{m}$  flux ratios would not apply to these last objects and our conclusion would be meaningless. However, there is no physical reason to believe that such a selection effect is present.

### *5.4 Contribution of different classes of sources to the X-ray background and the unified scheme*

The contribution to the XRB by a class of source with volume emissivity  $j(z)$  (which we

shall parametrize as  $j(z) = j_0 (1 + z)^{3+k}$ ,  $k = 0$  corresponding to no evolution) is

$$I = \frac{cH_0^{-1}}{4\pi} \int dz (1 + z)^{-5} (1 + \Omega_0 z)^{-\frac{1}{2}} j(z) K(z) \quad (19)$$

where  $K(z)$  is the K-correction (or simply  $(1 + z)^{-\alpha_X}$  for a power law spectrum of energy spectral index  $\alpha_X$ ) and  $\Omega_0$  is the density parameter. This relationship highlights on the relevance of the volume emissivity to computations of the background intensity contributed by different classes of sources.

While at soft energies  $E < 2$  keV either resolved (mainly AGN) or resolvable sources can account for  $\gtrsim 70\%$  of the XRB (Hasinger et al 1993; Barcons et al 1994) and they might in fact saturate it according to new ASCA measurements of the soft XRB intensity (Genderau et al. 1994), these sources probably yield  $< 20\%$  of the 2–10 keV XRB (Franceschini et al. 1993). These facts suggest the possibility that the sources dominating the hard XRB are silent at soft energies. In this vein, first Setti & Woltjer (1989) presented a model for the XRB based on highly absorbed AGN such those predicted by the unified scheme.

More detailed models based on the X-ray properties of unified schemes of AGN have been recently discussed by Comastri et al (1995) and Madau, Ghisellini & Fabian (1994). Both models assume that unobscured and obscured AGN evolve in luminosity  $L_X(z) = L_X(z = 0) \times (1 + z)^k$  with  $k \simeq 2.5 - 2.8$ . Taking into account the detailed response function of A2 we estimate the *equivalent* LXVE (see sect 4.3) of obscured objects with  $N_{HI} \geq 10^{22.5} \text{ cm}^{-2}$  implied by the model of Comastri et al (1995) amounts to about  $5 \times 10^{38} h_{50} \text{ erg s}^{-1} \text{ Mpc}^{-3}$  and to about  $4.5 \times 10^{38} h_{50} \text{ erg s}^{-1} \text{ Mpc}^{-3}$  for the model proposed by Madau et al (1994). Note that virtually no classified Seyfert 1 (or broad line object) has an absorbing column larger than  $10^{22.5} \text{ cm}^{-2}$  (Nandra & Pounds 1994, Turner & Pounds 1989) whereas almost all type 2 (or narrow line) objects display larger  $N_{HI}$  values.

The LXVE values of obscured objects in both models exceed by more than a factor of two the limit we computed summing up the 95% upper limits to the *equivalent* overall emissivity (LXVE  $\simeq 2 \times 10^{38} h_{50} \text{ erg s}^{-1} \text{ Mpc}^{-3}$ ) we have derived for Seyfert 2, HDGs and normal galaxies.

We believe that our limit is robust since the mid-IR selection should not be biased against X-ray sources (AGN or galaxies), even if strongly absorbed. Moreover the spectral sensitivity of the HEAO-1 A2 experiment well above 10 keV allows an exceptional capability to detect X-ray signals from the heavily extinguished ('hidden') AGN implied by the unification models. As previously admitted this does not invalidate the unification scheme since high enough absorption would reduce the hard X-ray flux.

However the constraint on models of the origin of the XRB is important, as it implies that the local population of absorbed or 'hidden' AGN is on average intrinsically too faint to yield the hard XRB if mild evolution is assumed as in the models of Comastri et al (1995) and Madau et al (1994). One possible alternative is to assume faster cosmological evolution for both unobscured and obscured AGN. But even assuming for both classes the fast evolution rates ( $k = 3.2 - 3.5$ ) found by Franceschini et al (1994) to fit the soft X-ray source counts and all the related statistics, would not solve the problem.

A further option would be that the evolution of 'hidden' AGN is faster than that of uncovered ones. In the unified scheme the faster evolution may be interpreted as the consequence of the increase of the average covering factor with increasing redshift.

Spectral evolution of the whole hard X-ray AGN population with an average column density increasing at increasing redshift as  $\log N_{HI} \sim 22 + 1.5(z/3.5)^{0.5}$  has indeed been invoked by Franceschini et al (1993) to explain the hard XRB and the soft and hard X-ray counts. This option may be inserted in the framework of the unified models as a case in which the average optical depth of the tori is decreasing with increasing cosmic time.

## 6. CONCLUSIONS

The extended galaxy  $12\mu\text{m}$  sample has proven to be extremely helpful in the study of the X-ray emission of extragalactic objects. The fact that most X-ray emitters are also  $12\mu\text{m}$  sources shows the importance of the study of the RMS sample. Moreover the spectral sensitivity of of the A1 and A2 experiments of the HEAO-1 mission have provided unique information about that numerous class of hard X-ray emitters predicted by the unified picture of AGN activity.

Our main conclusions can be summarized as follows:

1. Most of the local X-ray volume emissivity comes from Seyfert galaxies and in particular from Seyfert 1 galaxies.
2. The observed X-ray luminosity function at  $10^{42} \text{ erg s}^{-1} < L(2 - 10 \text{ keV}) < 10^{46} \text{ erg s}^{-1}$  can be mostly accounted for by  $12\mu\text{m}$  emitting AGN, under the assumption that a non-linear relation  $L_{12} \propto L_X^{0.8}$  with dispersion  $\langle \sigma[\log(L_X/L_{12})] \rangle \simeq 0.52$  holds.
3. The unified AGN scheme must be complemented with the additional item that the covering factor decreases with increasing source power.
4. Not many hidden AGN can exist unless their  $12\mu\text{m}$  is suppressed by some unexpected mechanism. There are at most 20% of hidden Seyfert 1 galaxies and at most 50% of hidden Seyfert 2 galaxies.
5. Presently available models of the XRB based on the unified scheme predict LXVEs much larger than that implied by our analysis of the hard X-ray data. However there are viable alternatives within the unified scheme.

In conclusion, we suggest that both the unified scheme of AGN activity and the proposed models for the synthesis of the XRB based on this scheme need to be complemented, in the former case by a luminosity dependence and in the later case by a redshift dependence.

We thank M. Persic and K. Jahoda for assistance in the use of the HEAO-1 A2 X-ray data. TM is grateful to Elihu Boldt for discussions. XB, AF, GDZ and LD acknowledge support by the European Union ‘Human Capital and Mobility’ program, under contract CHRX-CT92-0033. XB is partially supported by the DGICYT under project PB92-0501.

## REFERENCES

- Allen, J., Jahoda, K., Whitlock, L., 1994, *Legacy*, 5, 27
- Antonucci, R., 1993, *ARA&A*, 31, 473
- Antonucci, R.R.J., Miller, J., 1985, *ApJ*, 297, 621
- Avni, Y., Tananbaum, H., 1986, *ApJ*, 305, 83
- Awaki, H., Koyama, K., Inoue, H., Halpern, J.P., 1991, *PASJ*, 43, 195
- Band D.L., Malkan, M.A., 1989, *ApJ*, 345, 122
- Barcons, X., Branduardi-Raymont, G., Warwick, R.S., Fabian, A.C., Mason, K.O., McHardy, I.M., Rowan-Robinson, M., 1994, *MNRAS*, 268, 833
- Boldt, E., 1992, In: *The X-ray Background*, eds. Barcons, X., Fabian, A.C., Cambridge University Press, p. 115
- Boyle, B.J., Griffiths, R.E., Shanks, T., Stewart, G.C., Georgantopoulos, I., 1993, *MNRAS*, 260, 49
- Carrera, F.J. et al., 1993, *MNRAS*, 260, 376
- Carrera, F.J., Barcons, X., Butcher, J.A., Fabian, A.C., Lahav, O., Stewart, G.C., Warwick, R.S., 1995, *MNRAS*, in the press
- Cheng, F.Z., Danese, L., De Zotti, G., Lucchin, F., 1984, *MNRAS*, 208, 799
- Comastri, A., Setti, G., Zamorani, G., Hasinger, G., 1995, *A&A*, in the press
- Danese, L., Toffolatti, L., Franceschini, A., Martín-Mirones, J.M., De Zotti, G., 1993, *ApJ*, 412, 56
- de Grijp, M., Miley, G., Lub, J., de Jong, T., 1985, *Nat*, 314, 240
- De Zotti, G., Danese, L., Franceschini, A., Persic, M., Toffolatti, L., 1989, In: *Two Topics in X-ray Astronomy*, eds. Hunt, J., Battrick, B., ESA SP-296, p. 737
- Fabian, A.C., Barcons, X., 1992, *ARA&A*, 30, 429
- Franceschini, A., Martín-Mirones, J.M., Danese, L., De Zotti, G., 1993, *MNRAS*, 264, 35
- Franceschini, A., La Franca, F., Cristiani, S., Martín-Mirones, J.M., 1994, *MNRAS*, 269, 683
- Gendreau K.C., Bautz, M.W., Ricker, G.R., et al., 1995, *PASJ*, in the press

Granato, G. & Danese, L., 1994, MNRAS, 268, 235

Grossan, B.A., 1992, Ph. D. Thesis, Massachusetts Institute of Technology

Hasinger, G., Burg, R., Giacconi, R., Hartner, G., Schmidt, M., Trümper, J., Zamorani, G., 1993, A&A, 275, 1

Jahoda, K., Lahav, O., Mushotzky, R.F. & Boldt, E., 1991, ApJ, 378, L37

Jahoda, K., Lahav, O., Mushotzky, R.F. & Boldt, E., 1992, ApJ, 399, L107 (*Erratum*)

Krolik, J.H., Madau, P., Zycki, P.T., 1994, ApJ, 420, L57

Lahav, O., Fabian, A.C., Barcons, X., Boldt, E., Butcher, J., Carrera, F.J., Jahoda, K., Miyaji, T., Stewart, G.C., Warwick, R.S., 1993, Nat, 364, 693

Lawrence, A., 1991, MNRAS, 252, 586

Madau, P., Ghisellini, G., Fabian, A.C., 1994, MNRAS, 270, L17

Marshall, F.E., Boldt, E.A., Holt, S.S., et al., 1980, ApJ, 235, 4

Miyaji, T., Lahav, O., Jahoda, K., Boldt, E., 1994, ApJ, 434, 424

Mulchaey, J.S., Mushotzky, R.F., Weaver, K.A., 1992, ApJ, 390, L69

Nandra, K., Pounds, K.A., 1994, MNRAS, 268, 405

Piccinotti, G., Mushotzky, R.F., Boldt, E., Holt, S.S., Marshall, F.E., Serlemitsos, P.J., Shafer, R.A., 1982, ApJ, 253, 485

Pier E.A., Krolik, J.H., 1992, ApJ, 401, 99

Rush, B., Malkan, M.A., Spinoglio, L., 1993, ApJS, 89, 1

Setti, G., Woltjer, L., 1989, A&A, 224, L21

Turner, T.J., Pounds, K.A., 1989, MNRAS, 240, 833

Wood, K., Meckins, J., Yentis, D., et al, 1984, ApJS, 56, 507

## FIGURE CAPTIONS

FIG 1.– Far-Infrared colour-colour diagram for the RMS sources. Filled and open squares represent Seyfert 1 and 2 galaxies, respectively. Sources included in the Hot Dust Galaxy sample are marked with a triangle. Normal galaxies, starburst and narrow emission-line galaxies occupy a region confined around  $f_{100}/f_{12} \sim 30$  and  $f_{100}/f_{25} \sim 20$

FIG 2.– The  $12\mu\text{m}$  versus 5 keV monochromatic luminosity relation for the sample presented by Grossan (1992). Filled squares show actual data whilst triangles represent  $3\sigma$  upper limits to the  $12\mu\text{m}$  flux. The line is a non-linear fit, estimated using *survival* analysis techniques:  $\log L_X = -15.25 + 1.3 \log L_{12}$ .

FIG 3.– Total band X-ray intensity histograms around the various subsamples used (Seyfert 1, Seyfert 2, Hot Dust Galaxies, galaxies and whole sample). The hatched histogram represents the control sample histogram (i.e., blank sky measurements with the same geometry) for each case.

FIG 4.– Hard band X-ray intensity histograms around the Seyfert 1 and Seyfert 2 subsamples. The hatched histogram represents the control sample histogram (i.e., blank sky measurements with the same geometry) for each case.

FIG 5.– X-ray luminosity functions. Squares are from the sample by Grossan (1992), triangles by Piccinotti et al (1982). The hollow circles show the contribution from Seyfert 2 galaxies estimated from the A1 sample. The thick continuous line is the XLF predicted from the Seyfert 1 LF at  $12\mu\text{m}$  and a bivariate luminosity distribution, as discussed in Sect. 4.2. The dot-dashed line is the prediction for Seyfert 2s galaxies. The two thin continuous lines mark the 95% upper limit for the contribution of the normal galaxies and Hot Dust Galaxies.

FIG 6.– The  $12\mu\text{m}$  local luminosity function for Seyfert galaxies (filled circles), estimated from the IR sample of Rush et al. (1993). The LF of normal galaxies is shown for comparison. The continuous line shows a prediction based on the 2-10 XLF of Seyfert 1 estimated from the A1 sample (Grossan, 1992). See Sect. 4.2 for more details.